

# A New Group of Two-Dimensional Non-van der Waals Materials with Ultra Low Exfoliation Energies

Tom Barnowsky,<sup>†,‡</sup> Arkady V. Krasheninnikov,<sup>†,¶</sup> and Rico Friedrich<sup>\*,†,‡</sup>

<sup>†</sup>*Institute of Ion Beam Physics and Materials Research, Helmholtz-Zentrum  
Dresden-Rossendorf, 01328 Dresden, Germany*

<sup>‡</sup>*Theoretical Chemistry, Technische Universität Dresden, 01062 Dresden, Germany*

<sup>¶</sup>*Department of Applied Physics, Aalto University, Aalto 00076, Finland*

E-mail: [r.friedrich@hzdr.de](mailto:r.friedrich@hzdr.de)

## Abstract

The exfoliation energy — quantifying the energy required to extract a two-dimensional (2D) sheet from the surface of a bulk material — is a key parameter determining the synthesizability of 2D compounds. Here, using *ab initio* calculations, we present a new group of non-van der Waals 2D materials derived from non-layered crystals which exhibit ultra low exfoliation energies. In particular for sulfides, surface relaxations are essential to correctly describe the associated energy gain needed to obtain reliable results. Taking into account long-range dispersive interactions has only a minor effect on the energetics and ultimately proves that the exfoliation energies are close to the ones of traditional van der Waals bound 2D compounds. The candidates with the lowest energies, 2D SbTiO<sub>3</sub> and MnNaCl<sub>3</sub>, exhibit appealing electronic, potential topological, and magnetic features as evident from the calculated band structures making these systems an attractive platform for fundamental and applied nanoscience.

Keywords: 2D materials, exfoliation, computational materials science

The discovery of new two-dimensional (2D) materials — traditionally derived from bulk layered compounds held together by weak van der Waals (vdW) forces — outlined over the last two decades a diverse zoo of representatives showcasing unique topological,<sup>1</sup> electronic,<sup>2-4</sup> magnetic,<sup>5-7</sup> and superconducting<sup>8,9</sup> properties. The weak interaction between the structural units in their bulk counterparts leads to a natural geometric separation of the 2D subunits in the crystals, giving rise to the possibility of mechanical<sup>10</sup> and liquid-phase<sup>11</sup> exfoliation. This class of nanostructures thus opens up prospects for fundamental research in reduced dimensions as well as for various applications in the energy sector,<sup>12-14</sup> catalysis,<sup>15,16</sup> and opto-electronics.<sup>2,17,18</sup> The large scale deployment of these vdW 2D materials in modern technologies is, however, still very limited.<sup>19</sup>

In light of the ubiquitous use of many standard non-layered materials in research and technology for which handling and processing is well established, the search for non-vdW 2D materials is appealing.<sup>20</sup> Recently and somewhat unexpectedly, atomically thin 2D sheets derived from non-vdW bonded oxides were indeed manufactured. The first representatives realized in experiment by a special chemical exfoliation process were hematene<sup>21</sup> and ilmenene<sup>22</sup> obtained from the earth-abundant ores hematite ( $\alpha$ -Fe<sub>2</sub>O<sub>3</sub>) and ilmenite (FeTiO<sub>3</sub>), followed by a few others.<sup>23-36</sup> Unlike, *e.g.* silicene or borophene,<sup>37</sup> these materials do not need to strongly interact with a substrate to be stable. From the computational side, a recent data-driven search on non-vdW 2D systems outlined 28 candidates with a variety of appealing electronic and magnetic properties.<sup>38</sup> First application-oriented studies indicate promising perspectives for opto-electronics,<sup>39</sup> photo-catalytic activity for water splitting,<sup>21,22</sup> and photoconductivity.<sup>28</sup> Despite these early successes, the non-vdW 2D materials space is still very narrow and it remains to be understood what promotes the exfoliability of non-vdW bulk systems into 2D sheets.

A key quantity determining the synthesizability of 2D materials is the exfoliation energy  $\Delta E_{\text{exf}}$ . It represents the energy needed to peel off one 2D sheet from the surface of the bulk parent material. It can be computed accurately according to the method of Jung *et al.*<sup>40</sup> at minimal computational cost, who proved that the exfoliation energy is the energy difference between an isolated 2D sheet and one such facet in the bulk, also known as inter-layer binding energy. For the standard reference material graphene, the exfoliation energy is known to be  $\sim 20$  meV/Å<sup>2</sup> from both experiment and advanced density functional theory (DFT).<sup>41,42</sup> It was even found that this value appears to be universal for

many layered systems largely independent of their electronic structure. However, later on a rather complete screening of the vdW 2D materials space outlined a much wider distribution of exfoliation energies over several ten meV/Å<sup>2</sup>,<sup>43</sup> likely due to contributions from other interactions than just vdW. Based on detailed energetic and structural considerations, upper bounds of  $\sim 130$  meV/Å<sup>2</sup> and 200 meV/atom for the exfoliation energy have been proposed to consider a material as (classically) exfoliable.<sup>43,44</sup> As such, the calculated value of  $\sim 140$  meV/Å<sup>2</sup> ( $\sim 310$  meV/atom) for hematene<sup>38,45</sup> seems surprisingly high, yet successful liquid-phase isolation of the 2D sheet was reported.<sup>21</sup>

In the recent data-driven search for non-vdW 2D systems, it was indicated that for several of the 28 oxidic candidates, the exfoliation energy is significantly smaller. For a few systems, it even comes close to the one of graphene if the surface cations are in a low (+1) oxidation state<sup>38</sup> suggesting that mechanical peel-off might be feasible. This effect was rationalized through the minimization of electrostatic interactions between the 2D sheets in case of small surface charges. While the consideration of the systems in vacuum is an idealization with respect to experiment, it allows for an assessment of the fundamental exfoliation energetics of these materials. Here, we focus explicitly on novel candidates with surface cations in low oxidation states and generalize the previous efforts by investigating also non-oxides. The goal is to try to find an answer to the question: How small can the exfoliation energy of a non-vdW 2D material get?

The input structures are retrieved via the AFLOW APIs<sup>46–48</sup> and web interfaces<sup>49,50</sup> as well as the library of crystallographic prototypes.<sup>51</sup> The structures of Al<sub>2</sub>S<sub>3</sub> and MnNaCl<sub>3</sub> are depicted in Figs 1(a) and (b) as examples to visualize the structural prototype of the investigated systems. The exfoliated [001] facets are also indicated. The dynamic stability of the outlined 2D systems is verified as follows: First a 2×2 in-plane supercell is constructed from the relaxed structures. Then, the atomic coordinates are randomized (gaussian distribution, standard deviation 50 mÅ)<sup>52,53</sup> and the structures are reoptimized. In all cases, the slabs relax back to the previous geometry. Although they also exhibit the same structure, Yb<sub>2</sub>S<sub>3</sub> and Lu<sub>2</sub>S<sub>3</sub> are not considered here as the corresponding 2D sheets were found to be dynamically unstable during the test.

***Ab initio* Exfoliation Energies.** In Fig. 1(c), the calculated exfoliation energies are depicted also including, for comparison to the considered sulfides, the previously obtained values for the corresponding 2D oxides Al<sub>2</sub>O<sub>3</sub> and In<sub>2</sub>O<sub>3</sub>.<sup>38</sup> For the ternaries, the sheets can be terminated by either of the

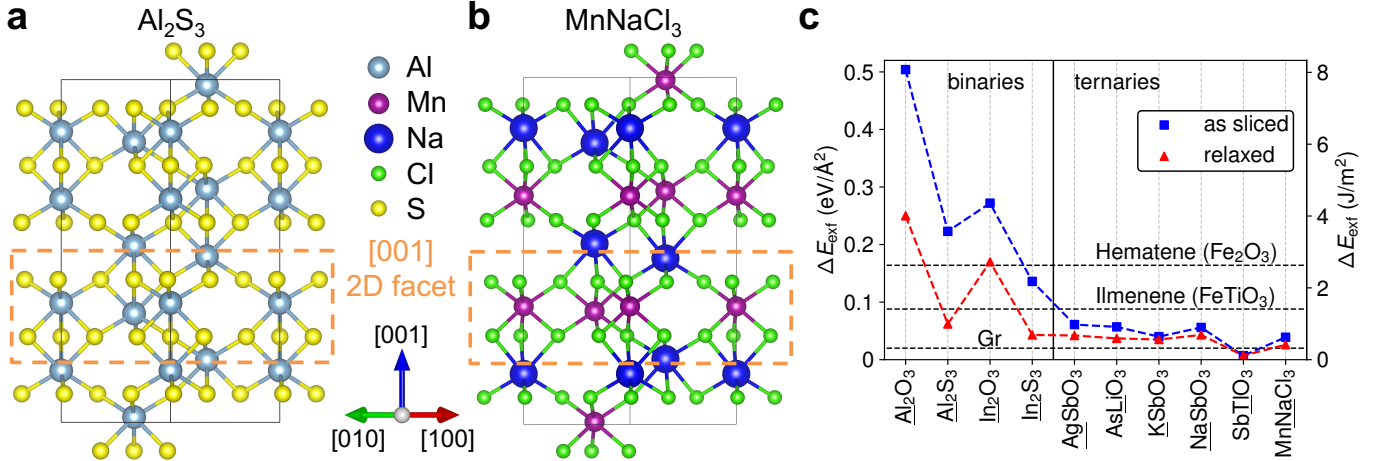


Figure 1: **Structures and exfoliation energies.** Atomic structure of (a)  $\text{Al}_2\text{S}_3$  and (b)  $\text{MnNaCl}_3$ .<sup>54</sup> The exfoliable [001] facet (monolayer) is indicated in the orange dashed box. The black line denotes the conventional unit cell. The compass indicating crystal directions applies to both figures. (c) Calculated exfoliation energies from SCAN without (as sliced) and with (relaxed) structural optimization of the 2D sheets. As a reference, the exfoliation energy of graphene (Gr)<sup>41,43</sup> as well as for hematene and ilmenene<sup>38</sup> are indicated by the dashed horizontal black lines. For the ternaries, the data for the slabs with the energetically favorable termination are plotted and for all systems, the terminating element is underlined at the bottom axis. The dashed lines connecting the data points are visual guides.

two cation species. Here, only the results for the energetically favorable termination are plotted and a comparison to the unpreferred termination is presented in Fig. S1 in the Supporting Information (SI). The  $\Delta E_{\text{exf}}$  of the newly considered systems extend over a large range of more than an order of magnitude. Ultra low values are achieved for the systems with surface cations in +1 oxidation states (such as  $\text{Ag}^+$ ,  $\text{Li}^+$ ,  $\text{K}^+$ ,  $\text{Na}^+$ , and  $\text{Tl}^+$ ) being as small as  $7 \text{ meV}/\text{\AA}^2$  for  $\text{SbTiO}_3$  and  $26 \text{ meV}/\text{\AA}^2$  for  $\text{MnNaCl}_3$ . These numbers are comparable to or even below the graphene reference value of  $\sim 20 \text{ meV}/\text{\AA}^2$ . They are significantly smaller than for any other non-vdW 2D system considered before.

The blue curve denotes the results obtained when omitting structural relaxations of the extracted 2D facets, *i.e.* keeping them “as sliced” from the bulk, as is common reliable practice for traditional vdW 2D systems.<sup>43</sup> These values reduce significantly for almost all candidates when including structural optimization as denoted by the red curve pinpointing at the crucial role of relaxations for the energetics of these materials. For the binary sulfides, this effect is particularly pronounced. Not only is the absolute value of the “relaxed” exfoliation energy of the sulfides a factor of four lower than for the corresponding oxides ( $62 \text{ meV}/\text{\AA}^2$  for  $\text{Al}_2\text{S}_3$  *vs.*  $250 \text{ meV}/\text{\AA}^2$  for  $\text{Al}_2\text{O}_3$  and  $43 \text{ meV}/\text{\AA}^2$  for  $\text{In}_2\text{S}_3$  *vs.*  $170 \text{ meV}/\text{\AA}^2$  for  $\text{In}_2\text{O}_3$ ), but also the relative change from “as sliced” to “relaxed” is much

stronger: While for the oxides the exfoliation energy reduces by about a factor of two upon relaxation (from  $504 \text{ meV}/\text{\AA}^2$  to  $250 \text{ meV}/\text{\AA}^2$  for  $\text{Al}_2\text{O}_3$  and from  $272 \text{ meV}/\text{\AA}^2$  to  $170 \text{ meV}/\text{\AA}^2$  for  $\text{In}_2\text{O}_3$ ), for the sulfides, it decreases by about a factor of three to four (from  $223 \text{ meV}/\text{\AA}^2$  to  $62 \text{ meV}/\text{\AA}^2$  for  $\text{Al}_2\text{S}_3$  and from  $136 \text{ meV}/\text{\AA}^2$  to  $43 \text{ meV}/\text{\AA}^2$  for  $\text{In}_2\text{O}_3$ ). For the other systems, the change in the values based on structural relaxations is less pronounced and amounts to maximally a factor of  $\sim 1.5$  (for  $\text{AsLiO}_3$  the reduction is from  $57 \text{ meV}/\text{\AA}^2$  to  $37 \text{ meV}/\text{\AA}^2$ ).

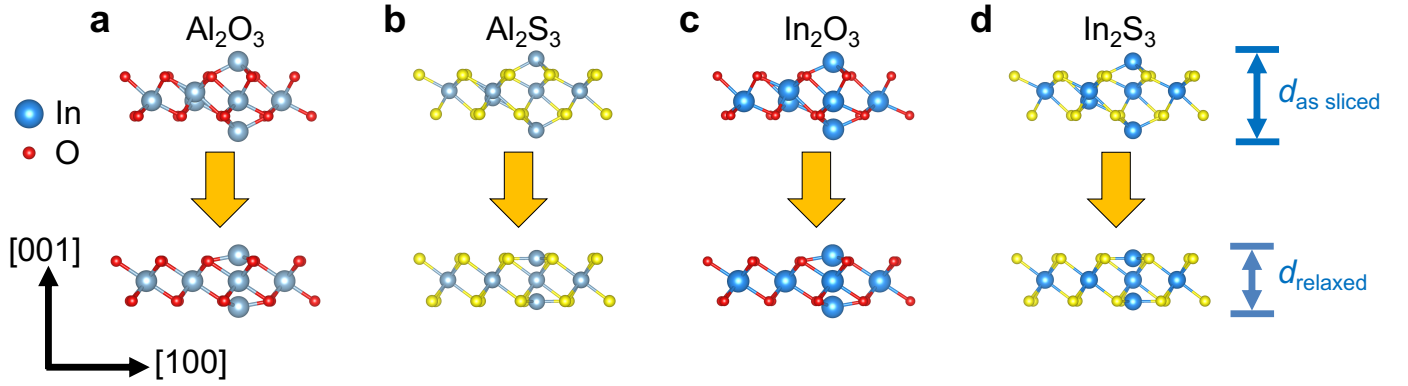


Figure 2: **Structural Relaxations.** Side view of the unit cells of “as sliced” (top) and “relaxed” (bottom) 2D (a)  $\text{Al}_2\text{O}_3$ , (b)  $\text{Al}_2\text{S}_3$ , (c)  $\text{In}_2\text{O}_3$ , and (d)  $\text{In}_2\text{S}_3$ .

**The Role of Structural Relaxations.** The origin of this strong change in energy in case of the sulfides as compared to the oxides can be traced back to intricate structural changes. The side views in Fig. 2 indicate that the 2D systems lower their energy by an inward relaxation of the terminating cations leading to an overall (vertical) thickness reduction from  $d_{\text{as sliced}}$  to  $d_{\text{relaxed}}$ . This effect is more pronounced in case of the sulfides as compared to the oxides. While  $\text{Al}_2\text{O}_3$  ( $\text{In}_2\text{O}_3$ ) relaxes from a thickness of  $3.84 \text{ \AA}$  ( $4.14 \text{ \AA}$ ) to  $2.72 \text{ \AA}$  ( $3.06 \text{ \AA}$ ),  $\text{Al}_2\text{S}_3$  ( $\text{In}_2\text{S}_3$ ) goes from  $4.94 \text{ \AA}$  ( $5.16 \text{ \AA}$ ) to  $2.96 \text{ \AA}$  ( $3.23 \text{ \AA}$ ). Hence, although the absolute thickness of the sulfides is larger, the absolute *reduction* by  $\sim 2 \text{ \AA}$  is about twice as large as for the oxides ( $\sim 1.1 \text{ \AA}$ ). Thus, the stronger structural relaxation due to the larger anion allows the surface cation to dive deeper into the anion plane leading to an almost planar coordination of the surface cations in the sulfides. Thereby, the energy is lowered more efficiently leading to stronger reductions in  $\Delta E_{\text{exf}}$ .

As a response to the vertical contraction, the oxides stretch laterally, *i.e.* the in-plane lattice constant of  $\text{Al}_2\text{O}_3$  ( $\text{In}_2\text{O}_3$ ) increases from  $4.75 \text{ \AA}$  ( $5.51 \text{ \AA}$ ) to  $4.86 \text{ \AA}$  ( $5.62 \text{ \AA}$ ). For the sulfides, this change is less pronounced as for  $\text{Al}_2\text{S}_3$  ( $\text{In}_2\text{S}_3$ ) the value goes from  $6.03 \text{ \AA}$  ( $6.59 \text{ \AA}$ ) to  $6.07 \text{ \AA}$  ( $6.59 \text{ \AA}$ ).

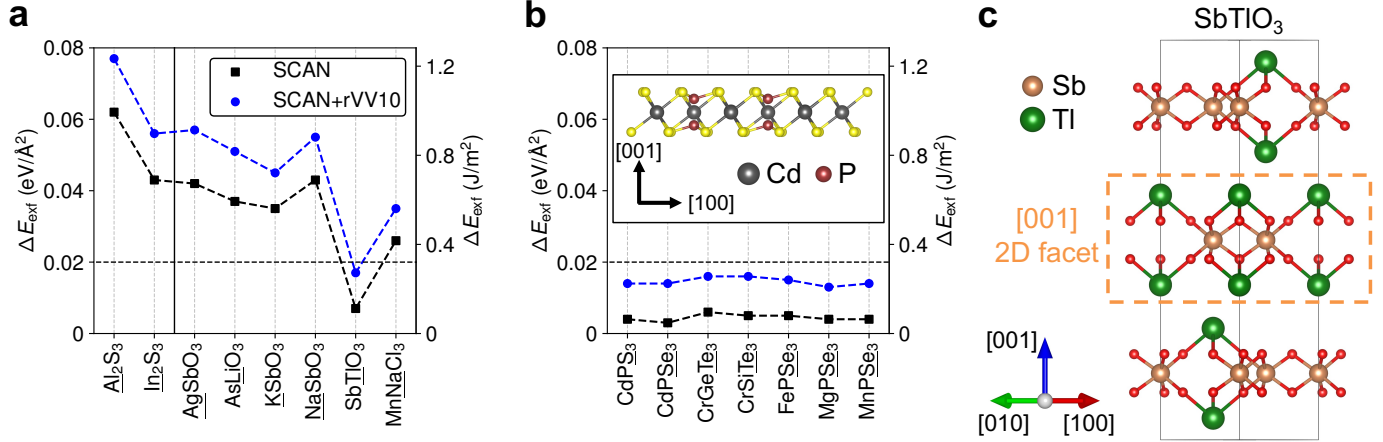


Figure 3: **Contribution of long-range vdW interactions.** Comparison of the calculated exfoliation energies from SCAN and SCAN+rVV10 for (a) the eight non-vdW 2D candidates and (b) seven vdW 2D systems with the same structure. The dashed horizontal black line indicates the graphene reference value.<sup>41,43</sup> The dashed lines connecting the data points are visual guides. Inset in (b): side view of  $\text{CdPS}_3$ . The vertical black line in (a) separates binaries from ternaries. (c) Atomic structure of  $\text{SbTlO}_3$ . The exfoliable [001] facet (monolayer) is indicated in the orange dashed box. The black line denotes the conventional unit cell.

**Contribution of Long-range vdW Interactions.** When exfoliation energies get as small as for graphene or even lower, the question of the importance of long-range vdW interactions naturally arises. While the employed SCAN functional has been pointed out to capture intermediate-range vdW interactions relevant for *e.g.* hydrogen bonds,<sup>55</sup> it does not include long-range dispersion contributions. These can be accounted for within the SCAN+rVV10 scheme.<sup>56</sup> We have thus also calculated the exfoliation energies for all systems with this approach and compare them to the plane SCAN results in Fig. 3(a). As expected, inclusion of the long-range interactions increases the exfoliation energies but only by a rather constant shift of 10-15 meV/Å<sup>2</sup> — the typical order of magnitude for dispersive interactions. Hence no qualitative change in the exfoliation behavior is anticipated from this.

As a further comparison, there are seven materials ( $\text{CdPS}_3$ ,  $\text{CdPSe}_3$ ,  $\text{CrGeTe}_3$ ,  $\text{CrSiTe}_3$ ,  $\text{FePSe}_3$ ,  $\text{MgPSe}_3$ , and  $\text{MnPSe}_3$ ) in the AFLOW database with the same structural prototype that are clearly layered, *i.e.* traditional vdW bonded materials as evident from visual inspection of the bulk geometries. Thus, the same structural prototype can host both vdW and non-vdW bonded 2D materials. The exfoliation energies for these well established 2D systems were also computed with the same methods and are provided in Fig. 3(b). Here, dispersive interactions are essential to obtain reliable absolute values as the constant shift by  $\sim 10$  meV/Å<sup>2</sup> increases the SCAN results by a factor of three. For the non-vdW systems in Fig. 3(a), the SCAN values account already for 70-80% of the SCAN+rVV10 result

since here the largest contribution to the bonding does not derive from long-range interactions. This consideration of the different interaction contributions therefore provides a clear distinction between non-vdW and vdW 2D materials.

SbTlO<sub>3</sub> is a special case at the intersection between the vdW and non-vdW 2D materials spaces. The optimized bulk (layered) structure with the exfoliable facet highlighted is depicted in Fig. 3(c). It is structurally equivalent to the other non-vdW systems as the Tl cations are at the surface of the 2D sheets in contrast to traditional 2D systems such as the ones from Fig. 3(b) which are terminated by the anions (see the side view of CdPS<sub>3</sub> in the inset as an example). Yet, the exfoliation energy of SbTlO<sub>3</sub> appears to be largely governed by long-range vdW contributions (see Fig. 3(a)). However, the intermediate range vdW interaction captured by the SCAN exfoliation energy accounts with  $\sim 40\%$  for a larger portion of the total exfoliation energy (from SCAN+rVV10) compared to the traditional vdW 2D compounds of Fig. 3(b) where this amounts on average to only  $\sim 30\%$ . As a result of these characteristics, this compound was already identified as a potential 2D material by Mounet *et al.*<sup>43</sup> although not discussed in detail.

An important general remark regarding the exfoliation energies must be made. While it is well known that the standard DFT functional PBE(+ $U$ ) tends to underestimate binding energies (overestimating bond lengths also known as underbinding, see also the comparison including the PBE+ $U$  exfoliation energies in Fig. SI2), there are several indications that the employed SCAN functional tends to overestimate covalent and ionic binding energy contributions (for oxides). Firstly, it has been shown that the SCAN results are usually very close to the exfoliation energies computed from LDA<sup>38</sup> for which overbinding effects are well established. Secondly, it has been demonstrated that SCAN systematically overestimates oxide formation enthalpies similar to LDA,<sup>57</sup> again indicating binding effects to be on the high side. SCAN+rVV10 was shown to compute long-range vdW contributions reliably with no particular bias with respect to standard reference results from the random phase approximation.<sup>56,58</sup> Thus, we expect the SCAN+rVV10 results to provide an upper bound for the exfoliation energies of non-vdW 2D materials.

**Band Structures and Magnetic Properties of SbTlO<sub>3</sub> and MnNaCl<sub>3</sub>.** To showcase the potential of these materials, we briefly discuss the band structure and magnetic properties of SbTlO<sub>3</sub> and MnNaCl<sub>3</sub> — the two systems with the lowest exfoliation energies — and present the results for

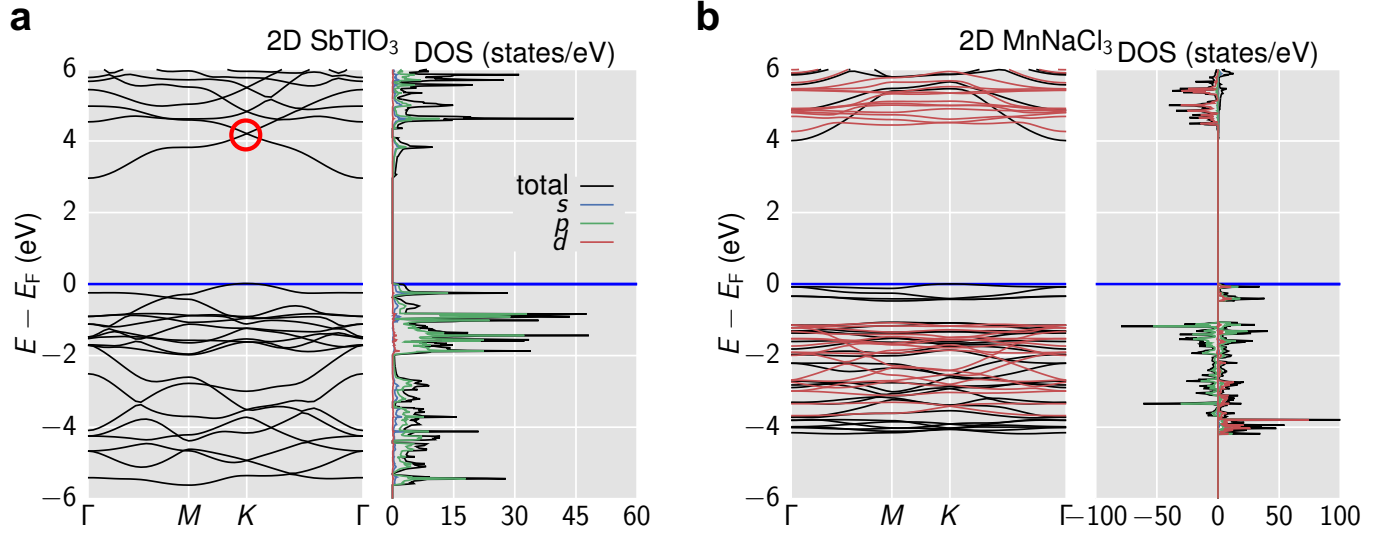


Figure 4: **Band structures and densities of states.** Band structure and density of states of (a) 2D  $\text{SbTiO}_3$  and (b) 2D  $\text{MnNaCl}_3$ . The energies are aligned at the respective Fermi energy  $E_F$ . For 2D  $\text{SbTiO}_3$ , a linear band crossing at the  $K$ -point is highlighted by the circle. For the spin polarized band structure in (b), majority spin bands (positive DOS) are indicated in black while minority spin bands (negative DOS) are in red.

all compounds in comparison to the respective bulk bands in the SI.

According to the band structures in Fig. 4, both systems are large gap insulators (calculated band gaps: 2.94 eV and 4.01 eV) with valence band maximum and conduction band minimum at the  $K$ - and  $\Gamma$ -points, respectively. An appealing feature for  $\text{SbTiO}_3$  is the Dirac cone like linear band crossing at the high-symmetry  $K$ -point at about 4.2 eV above the Fermi level which might be readily accessible via moderate doping. This feature might hint at interesting topological properties calling for further investigations for instance addressing the explicit calculation of topological invariants.  $\text{MnNaCl}_3$  on the other hand shows ferromagnetic coupling of the Mn moments amounting to  $\sim 4.6 \mu_B$ . The energy difference to the antiferromagnetic configuration is  $\sim 14$  meV/formula unit. This magnetic behavior is also reflected in the spin polarized bandstructure in Fig. 4(b) where both bands at the edges of the gap are derived from majority spin while minority spin states are separated by several hundred meV. In contrast to the previously reported magnetic non-vdW 2D candidates in Ref.,<sup>38</sup> the magnetic Mn ions are not at the surface of the slabs but in the interior (see also Fig. 1(b)). This is an important difference as the magnetic properties can be expected to be structurally better protected from environmental influences such as adsorbates. Based on the outlined electronic and magnetic characteristics, these



systems can thus reveal potential for *e.g.* optoelectronic and/or spintronic applications.

**Conclusions.** We have outlined a new group of non-vdW 2D materials exhibiting ultra low exfoliation energies — ultimately getting as small as the one of graphene. The investigated sulfides  $\text{Al}_2\text{S}_3$  and  $\text{In}_2\text{S}_3$  have exfoliation energies a factor of four smaller than the corresponding oxides, which can be traced back to exceptionally strong surface relaxations allowing for a significant energy gain. The smallest values close to the ones of traditional 2D systems are found for  $\text{SbTiO}_3$  and  $\text{MnNaCl}_3$ , as evident from the comparison to several vdW materials. The computed band structures of these most easily exfoliable compounds exhibit appealing electronic, possibly topological, and magnetic properties. Our results may thus be an important guide for extending the family of non-vdW 2D exfoliable systems representing a new class of low dimensional compounds and for studying their characteristics as well as applications.

## Methods

The *ab-initio* calculations are performed with AFLOW<sup>59,60</sup> and the Vienna *Ab-initio* Simulation Package (VASP)<sup>61–63</sup> employing the exchange-correlation functionals PBE,<sup>64</sup> SCAN,<sup>65</sup> SCAN+rVV10,<sup>56</sup> and PBE+ $U$ <sup>66–68</sup> with parameter choices in accordance with the AFLOW standard<sup>69</sup> as well as setting the internal VASPprecision to ACCURATE. For SCAN, projector-augmented-wave (PAW) pseudopotentials<sup>70</sup> of VASP version 5.4 are used and non-spherical contributions to the gradient of the density in the PAW spheres are included for SCAN and PBE+ $U$ . The [001] 2D facets are constructed from the bulk standard conventional unit cell with the respective AFLOW commands<sup>71</sup> resulting in structures with 10 atoms and including at least 20 Å of vacuum perpendicular to the slabs. For all facets, relaxation of both the ionic positions and the cell shape are carried out unless stated otherwise. The AFLOW internal automatic determination of  $k$ -point sets is used and for the calculations of the 2D facets, the setting for the number of  $k$ -points per reciprocal atom<sup>69</sup> is reduced to 1,000 resulting in  $\Gamma$ -centered  $10 \times 10 \times 1$  grids. The bandstructures are calculated for the optimized SCAN geometry using PBE(+ $U$ ) according to the AFLOW standard<sup>69</sup> as this functional has been successfully employed previously for the electronic properties of non-vdW 2D systems in Ref.<sup>38</sup> For computational efficiency, the dynamic stability check through the construction of  $2 \times 2$  in-plane supercells was carried out with

PBE(+ $U$ ).

The bulk and 2D candidate systems with expected magnetic ordering (MnNaCl<sub>3</sub>, CrGeTe<sub>3</sub>, CrSiTe<sub>3</sub>, FePSe<sub>3</sub>, and MnPSe<sub>3</sub>) are rigorously checked for magnetism using the algorithm developed within the CCE method,<sup>57,72</sup> *i.e.* investigating all possible FM and AFM configurations in the structural unit cell for five different sizes of induced magnetic moments each. In each case, the lowest energy magnetic state is used for the further calculations.

The exfoliation energy is computed as:

$$\Delta E_{\text{exf}} = \frac{E_{\text{slab}} - E_{\text{bulk}}}{A}, \quad (1)$$

where  $E_{\text{slab}}$  and  $E_{\text{bulk}}$  indicate the total energies of the relaxed 2D material and bulk, respectively and  $A$  is the in-plane surface area according to the relaxed bulk unit cell. As proven in Ref.,<sup>40</sup> the exfoliation energy from the surface of the material is exactly equal to the binding energy between layers/facets in the bulk.

Numerical data for the exfoliation energies are included in the Supporting Information.

## Acknowledgments

The authors thank the HZDR Computing Center, HLRS, Stuttgart, Germany and TU Dresden Cluster “Taurus” for generous grants of CPU time. R.F. acknowledges support from the Alexander von Humboldt foundation under the Feodor Lynen research fellowship. A.V.K. thanks the German Research Foundation (DFG) for the support through Project KR 4866/2-1 and the collaborative research center “Chemistry of Synthetic 2D Materials” SFB-1415-417590517. R.F. acknowledges Stefano Curtarolo and Agnieszka Kuc for fruitful discussions. The authors thank Mani Lokamani for technical support.

# Associated content

## Supporting Information Available

Exfoliation energies for different terminations for ternaries and for comparing results from different functionals, band structures for all binaries and ternaries compared to their bulk parent structures, and tables with numerical data.

## References

- (1) Kou, L.; Ma, Y.; Sun, Z.; Heine, T.; Chen, C. Two-Dimensional Topological Insulators: Progress and Prospects. *J. Phys. Chem. Lett.* **2017**, *8*, 1905–1919.
- (2) Butler, S. Z. et al. Progress, Challenges, and Opportunities in Two-Dimensional Materials Beyond Graphene. *ACS Nano* **2013**, *7*, 2898–2926.
- (3) Chhowalla, M.; Shin, H. S.; Eda, G.; Li, L.-J.; Loh, K. P.; Zhang, H. The chemistry of two-dimensional layered transition metal dichalcogenide nanosheets. *Nat. Chem.* **2013**, *5*, 263–275.
- (4) Manzeli, S.; Ovchinnikov, D.; Pasquier, D.; Yazyev, O. V.; Kis, A. 2D transition metal dichalcogenides. *Nat. Rev. Mater.* **2017**, *2*, 17033.
- (5) Burch, K. S.; Mandrus, D.; Park, J.-G. Magnetism in two-dimensional van der Waals materials. *Nature* **2018**, *563*, 47–52.
- (6) Gibertini, M.; Koperski, M.; Morpurgo, A. F.; Novoselov, K. S. Magnetic 2D materials and heterostructures. *Nat. Nanotechnol.* **2019**, *14*, 408–419.
- (7) Huang, Y. L.; Chen, W.; Wee, A. T. S. Two-dimensional magnetic transition metal chalcogenides. *SmartMat* **2021**, *2*, 139–153.
- (8) Cao, Y.; Fatemi, V.; Fang, S.; Watanabe, K.; Taniguchi, T.; Kaxiras, E.; Jarillo-Herrero, P. Unconventional superconductivity in magic-angle graphene superlattices. *Nature* **2018**, *556*, 43–50.

- (9) Campi, D.; Kumari, S.; Marzari, N. Prediction of Phonon-Mediated Superconductivity with High Critical Temperature in the Two-Dimensional Topological Semimetal W<sub>2</sub>N<sub>3</sub>. *Nano Lett.* **2021**, *21*, 3435–3442.
- (10) Novoselov, K. S.; Jiang, D.; Schedin, F.; Booth, T. J.; Khotkevich, V. V.; Morozov, S. V.; Geim, A. K. Two-dimensional atomic crystals. *Proc. Natl. Acad. Sci.* **2005**, *102*, 10451–10453.
- (11) Nicolosi, V.; Chhowalla, M.; Kanatzidis, M. G.; Strano, M. S.; Coleman, J. N. Liquid Exfoliation of Layered Materials. *Science* **2013**, *340*, 1226419.
- (12) Anasori, B.; Lukatskaya, M. R.; Gogotsi, Y. 2D metal carbides and nitrides (MXenes) for energy storage. *Nat. Rev. Mater.* **2017**, *2*, 16098.
- (13) Wang, J.; Malgras, V.; Sugahara, Y.; Yamauchi, Y. Electrochemical energy storage performance of 2D nanoarchitected hybrid materials. *Nat. Commun.* **2021**, *12*, 3563.
- (14) Chepkasov, I. V.; Ghorbani-Asl, M.; Popov, Z. I.; Smet, J. H.; Krasheninnikov, A. V. Alkali metals inside bi-layer graphene and MoS<sub>2</sub>: Insights from first-principles calculations. *Nano Energy* **2020**, *75*, 104927.
- (15) Deng, D.; Novoselov, K. S.; Fu, Q.; Zheng, N.; Tian, Z.; Bao, X. Catalysis with two-dimensional materials and their heterostructures. *Nat. Nanotechnol.* **2016**, *11*, 218–230.
- (16) Wang, Y.; Mao, J.; Meng, X.; Yu, L.; Deng, D.; Bao, X. Catalysis with Two-Dimensional Materials Confining Single Atoms: Concept, Design, and Applications. *Chem. Rev.* **2019**, *119*, 1806–1854.
- (17) Wang, Q. H.; Kalantar-Zadeh, K.; Kis, A.; Coleman, J. N.; Strano, M. S. Electronics and optoelectronics of two-dimensional transition metal dichalcogenides. *Nat. Nanotechnol.* **2012**, *7*, 699–712.
- (18) Lemme, M. C.; Li, L.-J.; Palacios, T.; Schwierz, F. Two-dimensional materials for electronic applications. *MRS Bull.* **2014**, *39*, 711–718.

- (19) Lemme, M. C.; Akinwande, D.; Huyghebaert, C.; Stampfer, C. 2D materials for future heterogeneous electronics. *Nat. Commun.* **2022**, *13*, 1392.
- (20) Balan, A. P. et al. Non-van der Waals quasi-2D materials; recent advances in synthesis, emergent properties and applications. *Mater. Today* **2022**,
- (21) Puthirath Balan, A. et al. Exfoliation of a non-van der Waals material from iron ore hematite. *Nat. Nanotechnol.* **2018**, *13*, 602–609.
- (22) Puthirath Balan, A. et al. A Non-van der Waals Two-Dimensional Material from Natural Titanium Mineral Ore Ilmenite. *Chem. Mater.* **2018**, *30*, 5923–5931.
- (23) Yadav, T. P.; Shirodkar, S. N.; Lertcumfu, N.; Radhakrishnan, S.; Sayed, F. N.; Malviya, K. D.; Costin, G.; Vajtai, R.; Yakobson, B. I.; Tiwary, C. S.; Ajayan, P. M. Chromiteen: A New 2D Oxide Magnetic Material from Natural Ore. *Adv. Mater. Interfaces* **2018**, *5*, 1800549.
- (24) Puthirath, A. B. et al. Scale-Enhanced Magnetism in Exfoliated Atomically Thin Magnetite Sheets. *Small* **2020**, *16*, 2004208.
- (25) Kaur, H.; Tian, R.; Roy, A.; McCrystal, M.; Horvath, D. V.; Lozano Onrubia, G.; Smith, R.; Ruether, M.; Griffin, A.; Backes, C.; Nicolosi, V.; Coleman, J. N. Production of Quasi-2D Platelets of Nonlayered Iron Pyrite ( $\text{FeS}_2$ ) by Liquid-Phase Exfoliation for High Performance Battery Electrodes. *ACS Nano* **2020**, *14*, 13418–13432.
- (26) Puthirath, A. B.; Balan, A. P.; Oliveira, E. F.; Sreepal, V.; Robles Hernandez, F. C.; Gao, G.; Chakingal, N.; Sassi, L. M.; Thibeorchews, P.; Costin, G.; Vajtai, R.; Galvao, D. S.; Nair, R. R.; Ajayan, P. M. Apparent Ferromagnetism in Exfoliated Ultrathin Pyrite Sheets. *J. Phys. Chem. C* **2021**, *125*, 18927–18935.
- (27) Moinuddin, M. G.; Srinivasan, S.; Sharma, S. K. Probing Ferrimagnetic Semiconductor with Enhanced Negative Magnetoresistance: 2D Chromium Sulfide. *Adv. Electron. Mater.* **2021**, *n/a*, 2001116.

- (28) Hu, L.; Cao, L.; Li, L.; Duan, J.; Liao, X.; Long, F.; Zhou, J.; Xiao, Y.; Zeng, Y.-J.; Zhou, S. Two-dimensional magneto-photoconductivity in non-van der Waals manganese selenide. *Mater. Horiz.* **2021**, *8*, 1286–1296.
- (29) Yousaf, A. et al. Exfoliation of Quasi-Two-Dimensional Nanosheets of Metal Diborides. *J. Phys. Chem. C* **2021**, *125*, 6787–6799.
- (30) Guo, Y.; Gupta, A.; Gilliam, M. S.; Debnath, A.; Yousaf, A.; Saha, S.; Levin, M. D.; Green, A. A.; Singh, A. K.; Wang, Q. H. Exfoliation of boron carbide into ultrathin nanosheets. *Nanoscale* **2021**, *13*, 1652–1662.
- (31) Gibaja, C. et al. Exfoliation of Alpha-Germanium: A Covalent Diamond-Like Structure. *Adv. Mater.* **2021**, *33*, 2006826.
- (32) Xu, J.; Li, W.; Zhang, B.; Zha, L.; Hao, W.; Hu, S.; Yang, J.; Li, S.; Gao, S.; Hou, Y. Free-standing 2D non-van der Waals antiferromagnetic hexagonal FeSe semiconductor: halide-assisted chemical synthesis and Fe<sup>2+</sup> related magnetic transitions. *Chem. Sci.* **2021**, *13*, 203–209.
- (33) Peng, J.; Liu, Y.; Lv, H.; Li, Y.; Lin, Y.; Su, Y.; Wu, J.; Liu, H.; Guo, Y.; Zhuo, Z.; Wu, X.; Wu, C.; Xie, Y. Stoichiometric two-dimensional non-van der Waals AgCrS<sub>2</sub> with superionic behaviour at room temperature. *Nat. Chem.* **2021**, *13*, 1235–1240.
- (34) Homkar, S.; Chand, B.; Rajput, S. S.; Gorantla, S.; Das, T.; Babar, R.; Patil, S.; Klingeler, R.; Nair, S.; Kabir, M.; Bajpai, A. Few-Layer SrRu<sub>2</sub>O<sub>6</sub> Nanosheets as Non-Van der Waals Honeycomb Antiferromagnets: Implications for Two-Dimensional Spintronics. *ACS Appl. Nano Mater.* **2021**, *4*, 9313–9321.
- (35) Chen, T. et al. Liquid phase exfoliation of nonlayered non-van der Waals iron trifluoride (FeF<sub>3</sub>) into 2D-platelets for high-capacity lithium storing cathodes. *FlatChem* **2022**, *33*, 100360.
- (36) Toksumakov, A. N.; Ermolaev, G. A.; Slavich, A. S.; Doroshina, N. V.; Sukhanova, E. V.; Yakubovsky, D. I.; Novikov, S. M.; Oreshonkov, A. S.; Tsybarenko, D. M.; Popov, Z. I.; Kvashnin, D. G.; Vyshnevyy, A. A.; Arsenin, A. V.; Ghazaryan, D. A.; Volkov, V. S. High-

refractive index and mechanically cleavable non-van der Waals InGaS<sub>3</sub>. 2022; <https://arxiv.org/abs/2205.02715>, arXiv:2205.02715.

- (37) Mannix, A. J.; Zhang, Z.; Guisinger, N. P.; Yakobson, B. I.; Hersam, M. C. Borophene as a prototype for synthetic 2D materials development. *Nat. Nanotechnol.* **2018**, *13*, 444–450.
- (38) Friedrich, R.; Ghorbani-Asl, M.; Curtarolo, S.; Krasheninnikov, A. V. Data-Driven Quest for Two-Dimensional Non-van der Waals Materials. *Nano Lett.* **2022**, *22*, 989–997.
- (39) Wei, Y.; Liu, C.; Wang, T.; Zhang, Y.; Qi, C.; Li, H.; Ma, G.; Liu, Y.; Dong, S.; Huo, M. Electronegativity regulation on opt-electronic properties of non van der Waals two-dimensional material: Ga<sub>2</sub>O<sub>3</sub>. *Comput. Mater. Sci.* **2020**, *179*, 109692.
- (40) Jung, J. H.; Park, C.-H.; Ihm, J. A Rigorous Method of Calculating Exfoliation Energies from First Principles. *Nano Lett.* **2018**, *18*, 2759–2765.
- (41) Zacharia, R.; Ulbricht, H.; Hertel, T. Interlayer cohesive energy of graphite from thermal desorption of polyaromatic hydrocarbons. *Phys. Rev. B* **2004**, *69*, 155406.
- (42) Björkman, T.; Gulans, A.; Krasheninnikov, A. V.; Nieminen, R. M. van der Waals Bonding in Layered Compounds from Advanced Density-Functional First-Principles Calculations. *Phys. Rev. Lett.* **2012**, *108*, 235502.
- (43) Mounet, N.; Gibertini, M.; Schwaller, P.; Campi, D.; Merkys, A.; Marrazzo, A.; Sohier, T.; Castelli, I. E.; Cepellotti, A.; Pizzi, G.; Marzari, N. Two-dimensional materials from high-throughput computational exfoliation of experimentally known compounds. *Nat. Nanotechnol.* **2018**, *13*, 246–252.
- (44) Choudhary, K.; Kalish, I.; Beams, R.; Tavazza, F. High-throughput Identification and Characterization of Two-dimensional Materials using Density functional theory. *Sci. Rep.* **2017**, *7*, 5179.
- (45) Wei, Y.; Ghorbani-Asl, M.; Krasheninnikov, A. V. Tailoring the Electronic and Magnetic Properties of Hematene by Surface Passivation: Insights from First-Principles Calculations. *J. Phys. Chem. C* **2020**, *124*, 22784–22792.

- (46) Taylor, R. H.; Rose, F.; Toher, C.; Levy, O.; Yang, K.; Buongiorno Nardelli, M.; Curtarolo, S. A RESTful API for exchanging materials data in the AFLOWLIB.org consortium. *Comput. Mater. Sci.* **2014**, *93*, 178–192.
- (47) Rose, F.; Toher, C.; Gossett, E.; Oses, C.; Buongiorno Nardelli, M.; Fornari, M.; Curtarolo, S. AFLUX: The LUX materials search API for the AFLOW data repositories. *Comput. Mater. Sci.* **2017**, *137*, 362–370.
- (48) Oses, C. et al. aflow++: a C++ framework for autonomous materials design. 2022; <http://arxiv.org/abs/2208.03052>.
- (49) Curtarolo, S.; Setyawan, W.; Wang, S.; Xue, J.; Yang, K.; Taylor, R. H.; Nelson, L. J.; Hart, G. L. W.; Sanvito, S.; Buongiorno Nardelli, M.; Mingo, N.; Levy, O. AFLOWLIB.ORG: A distributed materials properties repository from high-throughput *ab initio* calculations. *Comput. Mater. Sci.* **2012**, *58*, 227–235.
- (50) Esters, M.; Oses, C.; Divilov, S.; Eckert, H.; Friedrich, R.; Hicks, D.; Mehl, M. J.; Rose, F.; Smolyanyuk, A.; Calzolari, A.; Campilongo, X.; Toher, C.; Curtarolo, S. aflow.org: A Web Ecosystem of Databases, Software and Tools. 2022; <http://arxiv.org/abs/2207.09842>.
- (51) Mehl, M. J.; Hicks, D.; Toher, C.; Levy, O.; Hanson, R. M.; Hart, G. L. W.; Curtarolo, S. The AFLOW Library of Crystallographic Prototypes: Part 1. *Comput. Mater. Sci.* **2017**, *136*, S1–S828.
- (52) Bahn, S. R.; Jacobsen, K. W. An object-oriented scripting interface to a legacy electronic structure code. *Comput. Sci. Eng.* **2002**, *4*, 56–66.
- (53) Larsen, A. H. et al. The atomic simulation environment—a Python library for working with atoms. *J. Phys.: Condens. Matter* **2017**, *29*, 273002.
- (54) Momma, K.; Izumi, F. VESTA3 for three-dimensional visualization of crystal, volumetric and morphology data. *J. Appl. Crystallogr.* **2011**, *44*, 1272–1276.



- (55) Sun, J.; Remsing, R. C.; Zhang, Y.; Sun, Z.; Ruzsinszky, A.; Peng, H.; Yang, Z.; Paul, A.; Waghmare, U.; Wu, X.; Klein, M. L.; Perdew, J. P. Accurate first-principles structures and energies of diversely bonded systems from an efficient density functional. *Nat. Chem.* **2016**, *8*, 9.
- (56) Peng, H.; Yang, Z.-H.; Perdew, J. P.; Sun, J. Versatile van der Waals Density Functional Based on a Meta-Generalized Gradient Approximation. *Phys. Rev. X* **2016**, *6*, 041005.
- (57) Friedrich, R.; Usanmaz, D.; Oses, C.; Supka, A.; Fornari, M.; Buongiorno Nardelli, M.; Toher, C.; Curtarolo, S. Coordination corrected ab initio formation enthalpies. *npj Comput. Mater.* **2019**, *5*, 59.
- (58) Emrem, B.; Kempt, R.; Finzel, K.; Heine, T. London Dispersion-Corrected Density Functionals Applied to van der Waals Stacked Layered Materials: Validation of Structure, Energy, and Electronic Properties. *Adv. Theory Simul.* **2022**, *n/a*, 2200055.
- (59) Levy, O.; Chepulskii, R. V.; Hart, G. L. W.; Curtarolo, S. The New Face of Rhodium Alloys: Revealing Ordered Structures from First Principles. *J. Am. Chem. Soc.* **2010**, *132*, 833–837.
- (60) Curtarolo, S.; Setyawan, W.; Hart, G. L. W.; Jahnátek, M.; Chepulskii, R. V.; Taylor, R. H.; Wang, S.; Xue, J.; Yang, K.; Levy, O.; Mehl, M. J.; Stokes, H. T.; Demchenko, D. O.; Morgan, D. AFLOW: An automatic framework for high-throughput materials discovery. *Comput. Mater. Sci.* **2012**, *58*, 218–226.
- (61) Kresse, G.; Hafner, J. *Ab initio* molecular dynamics for liquid metals. *Phys. Rev. B* **1993**, *47*, 558–561.
- (62) Kresse, G.; Furthmüller, J. Efficient iterative schemes for *ab initio* total-energy calculations using a plane-wave basis set. *Phys. Rev. B* **1996**, *54*, 11169–11186.
- (63) Kresse, G.; Furthmüller, J. Efficiency of *ab-initio* total energy calculations for metals and semiconductors using a plane-wave basis set. *Comput. Mater. Sci.* **1996**, *6*, 15–50.
- (64) Perdew, J. P.; Burke, K.; Ernzerhof, M. Generalized Gradient Approximation Made Simple. *Phys. Rev. Lett.* **1996**, *77*, 3865–3868.

- (65) Sun, J.; Ruzsinszky, A.; Perdew, J. P. Strongly Constrained and Appropriately Normed Semilocal Density Functional. *Phys. Rev. Lett.* **2015**, *115*, 036402.
- (66) Dudarev, S. L.; Botton, G. A.; Savrasov, S. Y.; Humphreys, C. J.; Sutton, A. P. Electron-energy-loss spectra and the structural stability of nickel oxide: An LSDA+ $U$  study. *Phys. Rev. B* **1998**, *57*, 1505–1509.
- (67) Liechtenstein, A. I.; Anisimov, V. I.; Zaanen, J. Density-functional theory and strong interactions: Orbital ordering in Mott-Hubbard insulators. *Phys. Rev. B* **1995**, *52*, R5467–R5470.
- (68) Anisimov, V. I.; Zaanen, J.; Andersen, O. K. Band theory and Mott insulators: Hubbard  $U$  instead of Stoner  $I$ . *Phys. Rev. B* **1991**, *44*, 943–954.
- (69) Calderon, C. E.; Plata, J. J.; Toher, C.; Oses, C.; Levy, O.; Fornari, M.; Natan, A.; Mehl, M. J.; Hart, G. L. W.; Buongiorno Nardelli, M.; Curtarolo, S. The AFLOW standard for high-throughput materials science calculations. *Comput. Mater. Sci.* **2015**, *108 Part A*, 233–238.
- (70) Kresse, G.; Joubert, D. From ultrasoft pseudopotentials to the projector augmented-wave method. *Phys. Rev. B* **1999**, *59*, 1758–1775.
- (71) Chepulskii, R. V.; Curtarolo, S. First principles study of Ag, Au, and Cu surface segregation in FePt-L1<sub>0</sub>. *Appl. Phys. Lett.* **2010**, *97*, 221908.
- (72) Friedrich, R.; Esters, M.; Oses, C.; Ki, S.; Brenner, M. J.; Hicks, D.; Mehl, M. J.; Toher, C.; Curtarolo, S. Automated coordination corrected enthalpies with AFLOW-CCE. *Phys. Rev. Mater.* **2021**, *5*, 043803.

# A New Group of Two-Dimensional Non-van der Waals Materials with Ultra Low Exfoliation Energies

## Supporting Information

Tom Barnowsky,<sup>1,2</sup> Arkady V. Krasheninnikov,<sup>1,3</sup> and Rico Friedrich<sup>1,2,\*</sup>

<sup>1</sup>*Institute of Ion Beam Physics and Materials Research,*

*Helmholtz-Zentrum Dresden-Rossendorf, 01328 Dresden, Germany*

<sup>2</sup>*Theoretical Chemistry, Technische Universität Dresden, 01062 Dresden, Germany*

<sup>3</sup>*Department of Applied Physics, Aalto University, Aalto 00076, Finland*

(Dated: September 26, 2022)

### I. Comparing exfoliation energies of ternary systems with different terminations

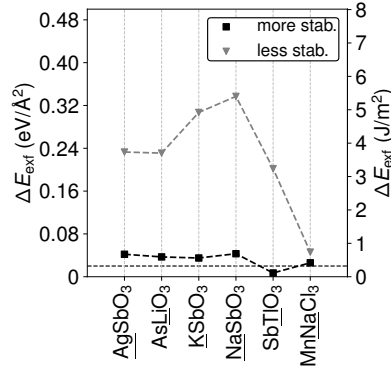


FIG. S1. **Exfoliation energies for different terminations for ternary systems.** The terminating elements for the energetically more stable slabs are underlined. As a reference, the exfoliation energy of graphene [1, 2] is indicated by the dashed black line. The dashed lines connecting the data points are visual guides.

Fig. S1 shows the exfoliation energies for the energetically preferred (more stable) and unfavored (less stable) termination for ternaries. Due to the large difference in the oxidation states of the surface cations for the first five systems (+1 vs. +5) the values vary by a factor five to almost 30 for the different terminations. For MnNaCl<sub>3</sub>, the change is less pronounced since due to the Cl<sup>-</sup> anions, the inner Mn is assigned the oxidation state +2.

### II. Comparing exfoliation energies from different functionals

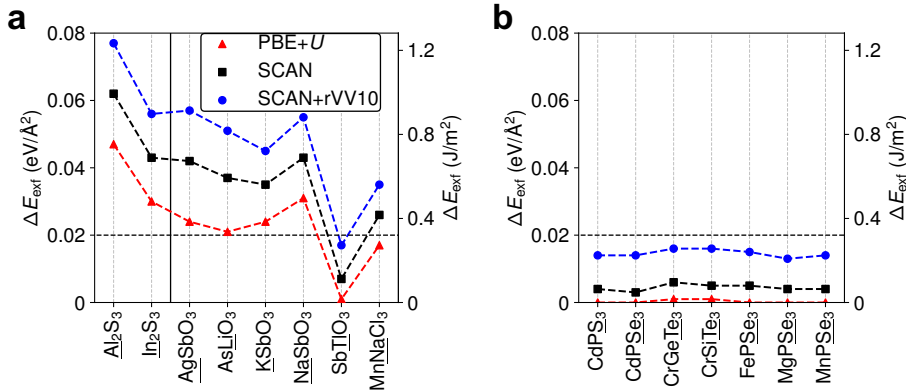


FIG. S2. **Comparison of exfoliation energies.** Exfoliation energies for different functionals for (a) the eight non-vdW 2D candidates and (b) seven vdW 2D systems with the same structure. Note that in case of Al<sub>2</sub>S<sub>3</sub>, AsLiO<sub>3</sub>, KSbO<sub>3</sub>, NaSbO<sub>3</sub>, and SbTiO<sub>3</sub> PBE+*U* reduces to PBE according to the standard workflow of AFLOW. As a reference, the exfoliation energy of graphene [1, 2] is indicated by the dashed horizontal black line. The dashed lines connecting the data points are visual guides.

\* r.friedrich@hzdr.de

### III. Band structures and densities of states

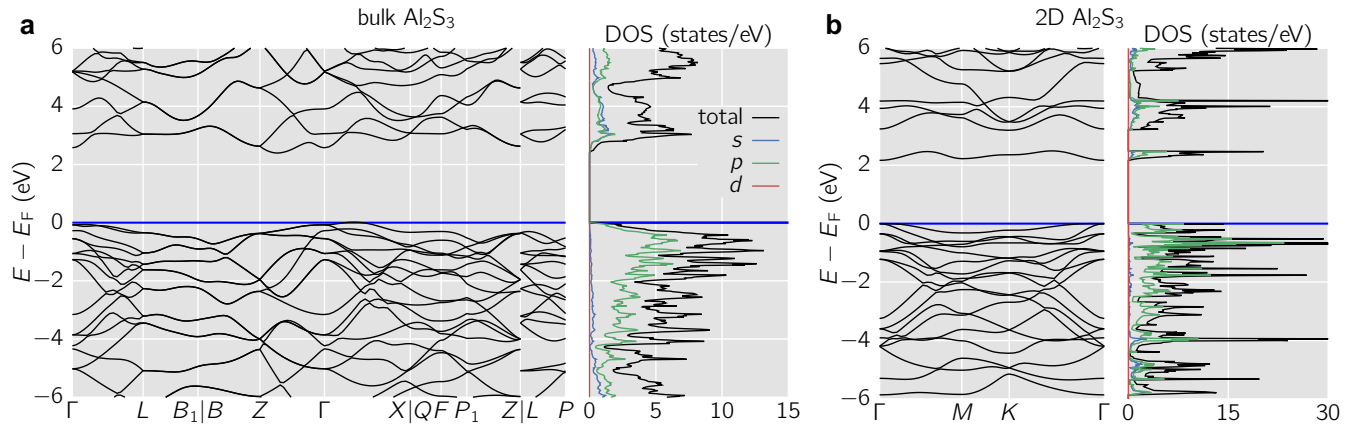


FIG. S3. Bandstructure and density of states for bulk (a) and 2D (b)  $\text{Al}_2\text{S}_3$ . The energies are aligned at the respective Fermi energy  $E_F$ .

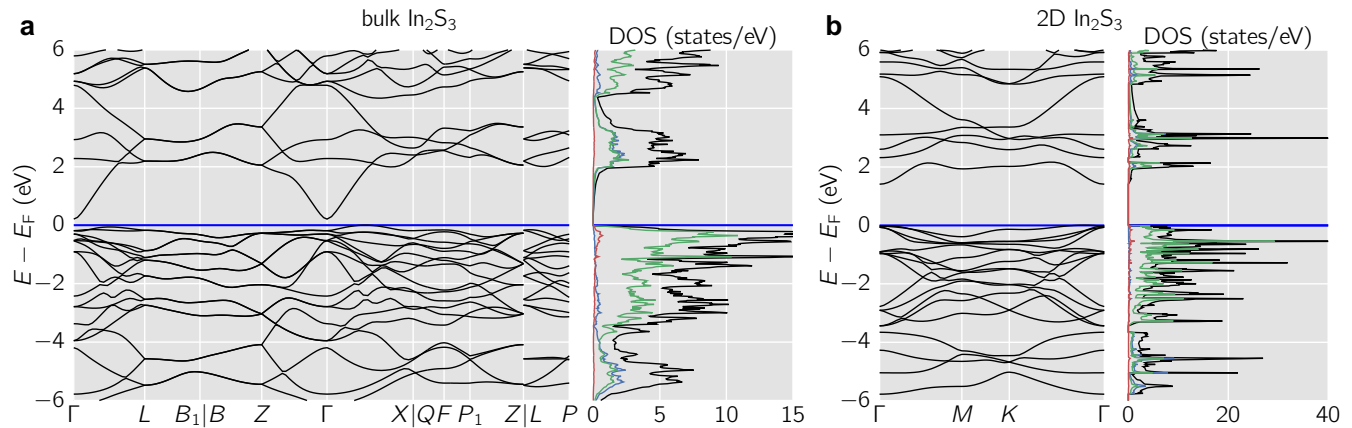


FIG. S4. Bandstructure and density of states for bulk (a) and 2D (b)  $\text{In}_2\text{S}_3$ . The energies are aligned at the respective Fermi energy  $E_F$ .

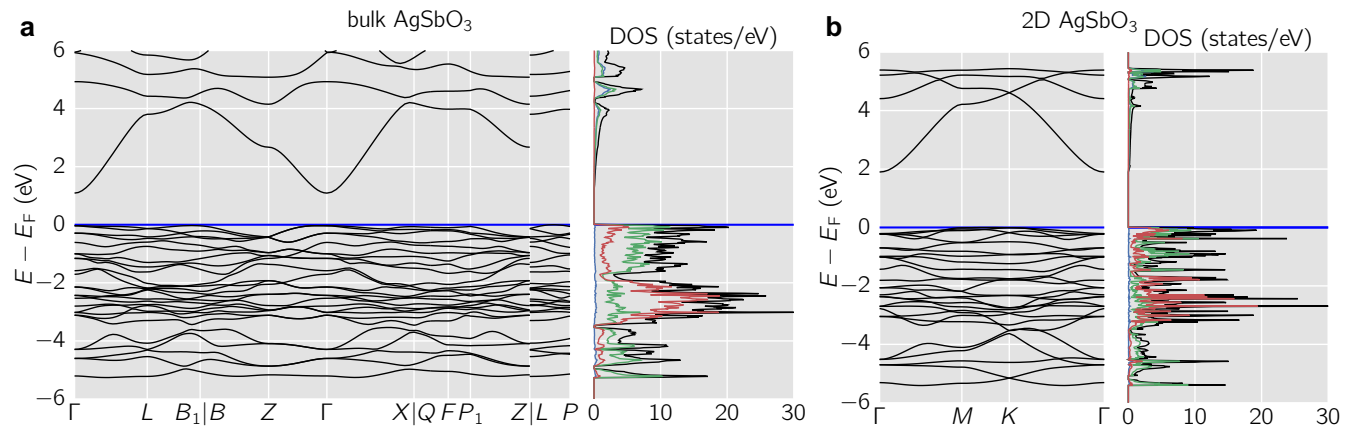


FIG. S5. Bandstructure and density of states for bulk (a) and 2D (b)  $\text{AgSbO}_3$ . The energies are aligned at the respective Fermi energy  $E_F$ . For the spin polarized bandstructure, majority spin bands (positive DOS) are indicated in black while minority spin bands (negative DOS) are in red.

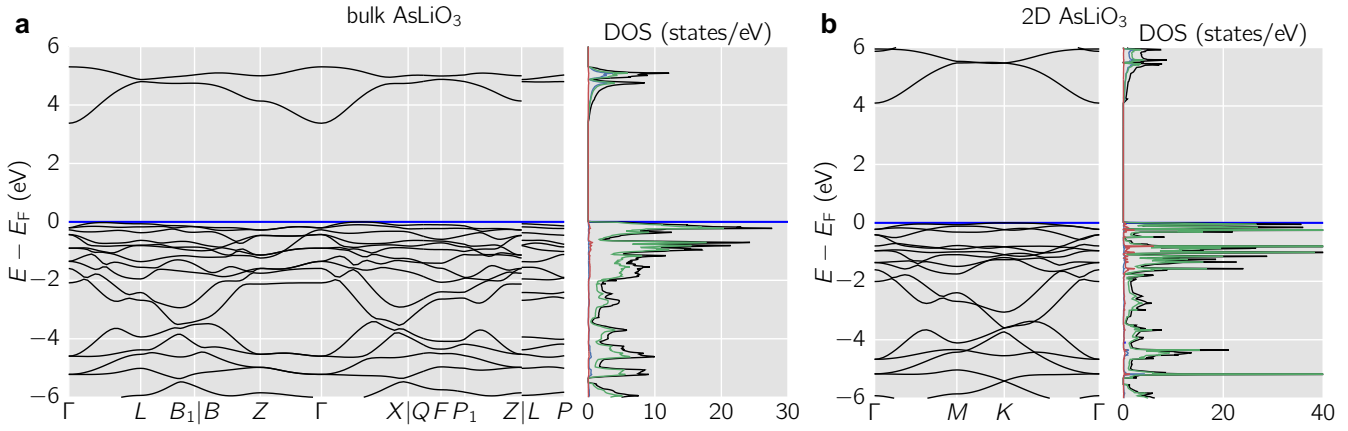


FIG. S6. Bandstructure and density of states for bulk (a) and 2D (b)  $\text{AsLiO}_3$ . The energies are aligned at the respective Fermi energy  $E_F$ .

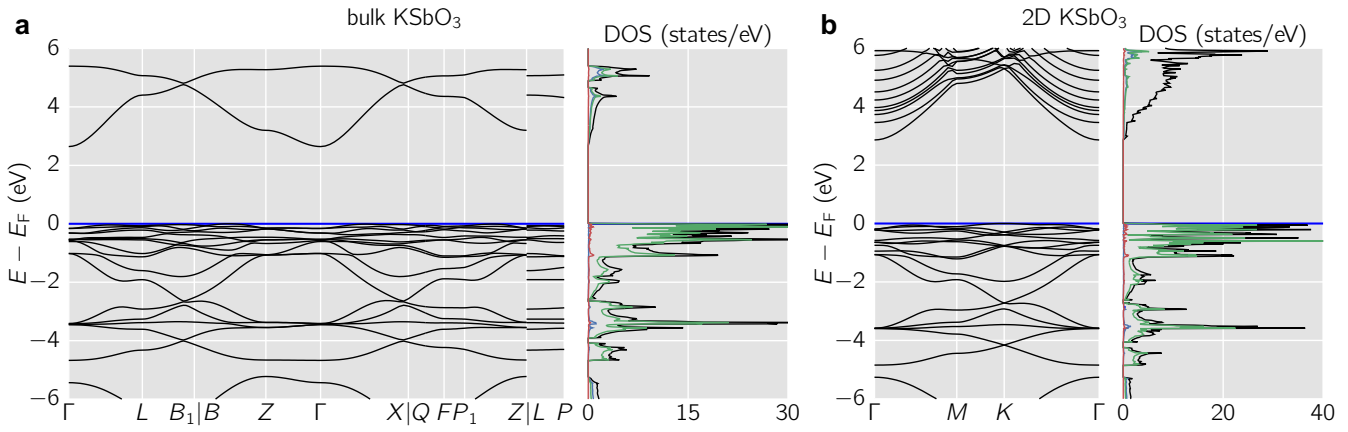


FIG. S7. Bandstructure and density of states for bulk (a) and 2D (b)  $\text{KSbO}_3$ . The energies are aligned at the respective Fermi energy  $E_F$ .

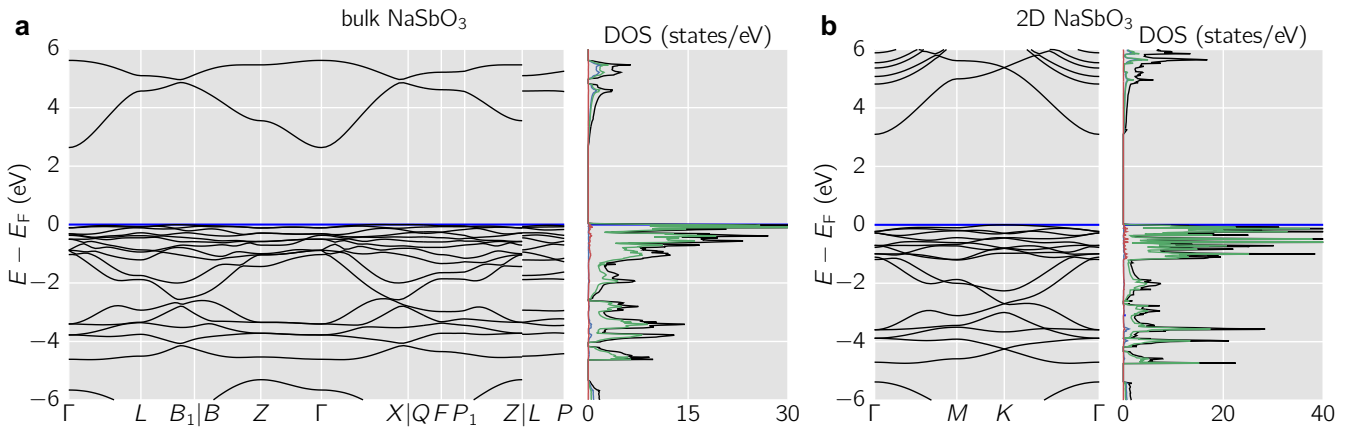


FIG. S8. Bandstructure and density of states for bulk (a) and 2D (b)  $\text{NaSbO}_3$ . The energies are aligned at the respective Fermi energy  $E_F$ .

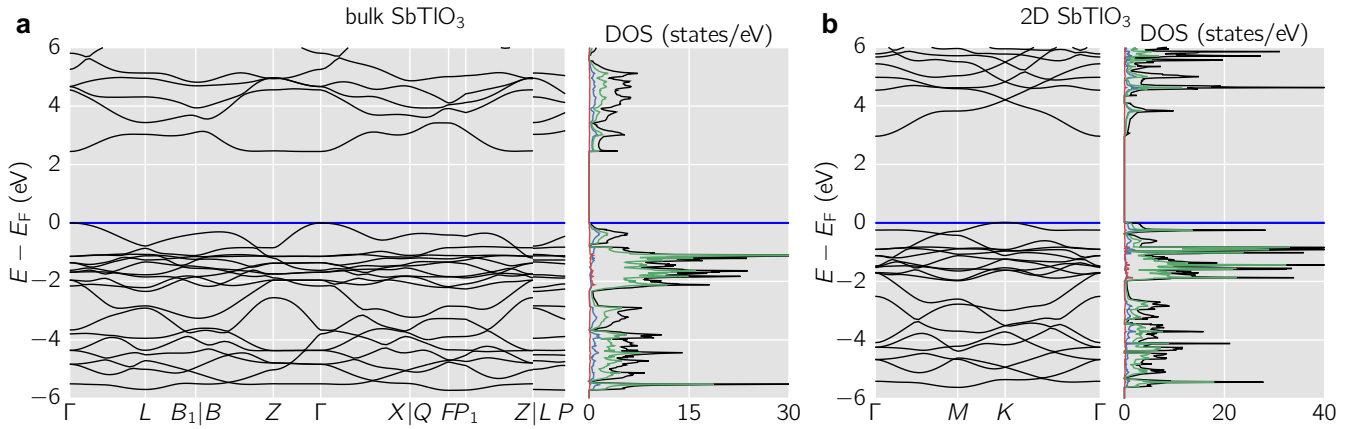


FIG. S9. Bandstructure and density of states for bulk (a) and 2D (b)  $\text{SbTiO}_3$ . The energies are aligned at the respective Fermi energy  $E_F$ .

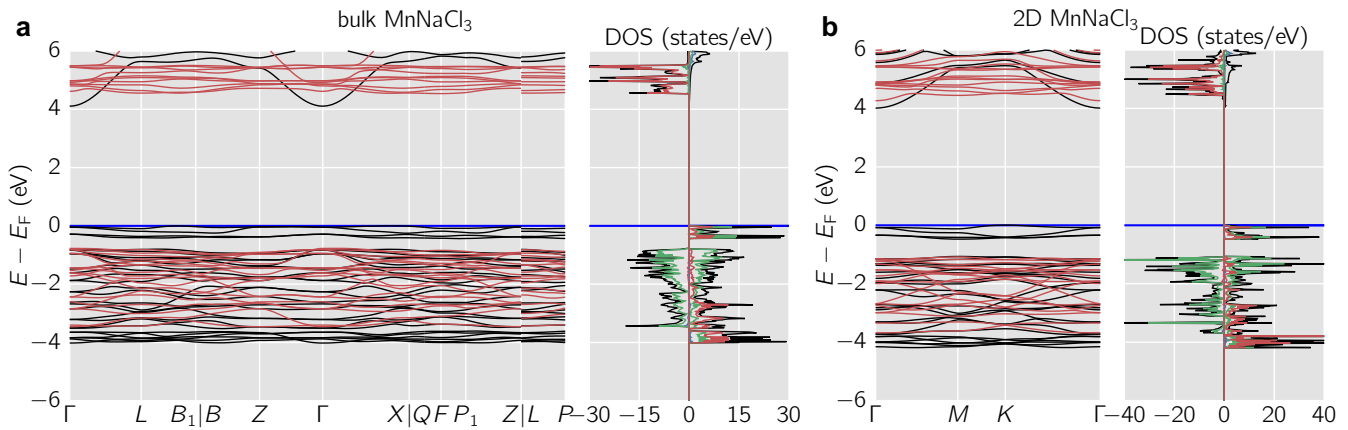


FIG. S10. Bandstructure and density of states for bulk (a) and 2D (b)  $\text{MnNaCl}_3$ . The energies are aligned at the respective Fermi energy  $E_F$ . For the spin polarized bandstructure, majority spin bands (positive DOS) are indicated in black while minority spin bands (negative DOS) are in red.

#### IV. Tables with numerical data

TABLE I: **Exfoliation energies for binaries.** Exfoliation energies for the binaries calculated with different functionals from only a static (“as sliced”) electronic calculation as well as when relaxing the ionic positions and (in-plane) cell parameters of the 2D materials. Note that in case of  $\text{Al}_2\text{S}_3$  PBE+ $U$  reduces to PBE according to the standard workflow of AFLOW. All values are in  $\text{eV}/\text{\AA}^2$ .

formula	PBE(+ $U$ )		SCAN		SCAN+rVV10	
	static	rel. ions and cell	static	rel. ions and cell	static	rel. ions and cell
$\text{Al}_2\text{S}_3$	0.196	0.047	0.223	0.062	0.237	0.077
$\text{In}_2\text{S}_3$	0.114	0.030	0.136	0.043	0.149	0.056

TABLE II: **Exfoliation energies for ternaries.** Exfoliation energies for the ternary systems calculated with different functionals for fully relaxing all systems, *i.e.* the ionic positions and the (in-plane) cell parameters. The data for the energetically preferred (more stab.) cation termination are given. For SCAN, also the values from only a static (“as sliced”) electronic calculation and the energetically less preferred (less stab.) cation termination are included. Note that in case of AsLiO<sub>3</sub>, KSbO<sub>3</sub>, NaSbO<sub>3</sub>, SbTiO<sub>3</sub>, and MgPSe<sub>3</sub> PBE+*U* reduces to PBE according to the standard workflow of AFLOW. All values are in eV/Å<sup>2</sup>.

compound	PBE(+ <i>U</i> )		SCAN		SCAN+rVV10	compound	PBE(+ <i>U</i> )		SCAN	SCAN+rVV10
	more stab.	more stab. static	more stab. rel. ions and cell	less stab. rel. ions and cell	more stab.					
AgSbO <sub>3</sub>	0.024	0.061	0.042	0.233	0.057	CdPS <sub>3</sub>	0	0.004		0.014
AsLiO <sub>3</sub>	0.021	0.057	0.037	0.231	0.051	CdPSe <sub>3</sub>	0	0.003		0.014
KSbO <sub>3</sub>	0.024	0.040	0.035	0.307	0.045	CrGeTe <sub>3</sub>	0.001	0.006		0.016
NaSbO <sub>3</sub>	0.031	0.056	0.043	0.337	0.055	CrSiTe <sub>3</sub>	0.001	0.005		0.016
SbTiO <sub>3</sub>	0.001	0.007	0.007	0.202	0.017	FePSe <sub>3</sub>	0	0.005		0.015
MnNaCl <sub>3</sub>	0.017	0.039	0.026	0.046	0.035	MgPSe <sub>3</sub>	0	0.004		0.013
						MnPSe <sub>3</sub>	0	0.004		0.014

## REFERENCES

- 
- [1] R. Zacharia, H. Ulbricht, and T. Hertel, *Interlayer cohesive energy of graphite from thermal desorption of polyaromatic hydrocarbons*, Phys. Rev. B **69**, 155406 (2004).
- [2] N. Mounet, M. Gibertini, P. Schwaller, D. Campi, A. Merkys, A. Marrazzo, T. Sohier, I. E. Castelli, A. Cepellotti, G. Pizzi, and N. Marzari, *Two-dimensional materials from high-throughput computational exfoliation of experimentally known compounds*, Nat. Nanotechnol. **13**, 246–252 (2018).